Drop Mass Transfer in a Microfluidic Chip Compared to a Centrifugal Contactor

Martin B. Nemer, Christine C. Roberts, Lindsey G. Hughes, Nicholas B. Wyatt, Carlton F. Brooks, and Rekha Rao
Sandia National Laboratories, Albuquerque, NM 87123

DOI 10.1002/aic.14510
Published online June 13, 2014 in Wiley Online Library (wileyonlinelibrary.com)

A model system was developed for enabling a multiscale understanding of centrifugal-contactor liquid–liquid extraction. The system consisted of Nd(III) + xylenol orange in the aqueous phase buffered to pH = 5.5 by KHP, and dodecane + thenoyltrifluroroacetone (HTTA) + tributyphosphate (TBP) in the organic phase. Diffusion constants were measured for neodymium in both the organic and aqueous phases, and the Nd(III) partition coefficients were measured at various HTTA and TBP concentrations. A microfluidic channel was used as a high-shear model environment to observe mass transfer on a droplet scale with xylenol orange as the aqueous-phase metal indicator; mass-transfer rates were measured quantitatively in both diffusion and reaction limited regimes on the droplet scale. The microfluidic results were comparable to observations made for the same system in a laboratory scale liquid–liquid centrifugal contactor, indicating that single drop microfluidic experiments can provide information on mass transfer in complicated flows and geometries. © 2014 American Institute of Chemical Engineers *AIChE J*, 60: 3071–3078, 2014
Keywords: separation techniques, extraction, microfluidics

Introduction

Centrifugal contactors are used for specialized liquid–liquid extraction processes in the chemical, nuclear, and biotechnology industries. In nuclear waste reprocessing, they are uniquely suited for liquid–liquid extraction to separate out the reusable fuel from spent fuel rods, to separate out isotopes to optimize disposal methods, and to separate rare-earth elements. Each contactor acts as a stage of the separation process, but is physically isolated except for inflow and outflow streams; thus issues of monitoring and troubleshooting issue are improved compared to a monolithic column.

In a centrifugal contactor, two immiscible liquids are mixed at high speeds using a rotor, which creates a fine dispersion of droplets of one fluid in the other. High shear rates and large interfacial area between the two liquids creates an efficient environment for mass transfer of species from one fluid to another. The internal portion of the rotor also acts as a centrifuge, so that the emulsion is broken, and the organic and aqueous phases are separated from each other into two outlet streams.

Significant progress has been made to understand the fluid mechanics and mass transport in centrifugal contactors through modeling[1–3] and laboratory scale experiments.[4–9] In order to fully understand such studies, however, fundamental parameters are necessary such as the droplet size and distribution, mass-transfer coefficients, diffusion coefficients, and partition coefficients. Established methods exist for obtaining diffusion coefficients, for example, using a side-by-side diffusion cell.[10,11] Partition coefficients can also be measured with accuracy[12]; however, mass transfer greatly depends on mixing speeds, interfacial area, and the existence of boundary layers, making its measurement nontrivial. In cases where it is infeasible to directly measure mass-transfer coefficients, inverse methods may be applicable.[13]

To obtain mass-transfer coefficients that are relevant for the centrifugal contactor, it is best to use a model environment that also experiences high shear. One such controlled environment is that within a microfluidic chip. Microfluidic devices have proven useful for observing mass transfer quantitatively on a single drop basis.[14–17] Microfluidic devices are ideal model environments since they can produce high mixing speeds with known interfacial areas.[14] Reliable production of monodisperse oil in water and water in oil droplets has been well documented for a variety of channel geometries.[18–20] Unlike falling droplet experiments where motion is driven by gravity,[21,22] residence and reaction times for droplets in microfluidic channels are on the order of those observed for centrifugal contactors. Microfluidic devices have also been used to characterize the effects of surfactant on the drop interface.[23,24] By observing the circulation in droplets, information pertaining to slip at the liquid–liquid interface and Marangoni stresses can be elucidated.

Here, a system that mimics the TRUEX[25] liquid–liquid extraction process, where transuranic metals are separated

Sandia National Laboratories is a multiprogram laboratory managed and operated by Sandia Corporation, a wholly owned subsidiary of Lockheed Martin Corporation, for the U.S. Department of Energy's National Nuclear Security Administration under contract DE-AC04-94AL85000.

Additional Supporting Information may be found in the online version of this article.

Corresponding author concerning this article should be addressed to M. B. Nemer at mbnemer@sandia.gov.

from nuclear waste, is studied in a microfluidic chip and in a contactor. The goal of this work was to develop a model system whereby the mass transfer could be observed in real time within the microfluidic chip and then compared to the contactor results. The extraction of neodymium (Nd^{3+}) from aqueous droplets to dodecane using the complexant thenoyltrifluoroacetone (HTTA) and ligand tri-*n*-butyl phosphate (TBP) was chosen as a model mass-transfer system. The aqueous phase also included xylenol orange as an indicator for Nd^{3+}. The reaction for an analogous system using carbon tetrachloride as the organic phase was found to be[12]

$$Nd^{3+}(aq)+3\ HTTA(o)+2\ TBP(o) \leftrightarrow Nd(TTA)_3(TBP)_2(o)+3\ H^+(aq). \quad (1)$$

However, as shown in Section (Results, Partition Coefficients), it appears from the partition data that more than one complex is being formed at pH = 5.5.

Parameters including diffusion and distribution coefficients were obtained to better understand the contactor behavior. A flow focusing microfluidic channel is used to observe mass transfer and measure mass-transfer coefficients on a single drop basis. In a separate work, flow inside of the droplets was measured to determine whether TBP, a surface active material, may affect the internal circulation.[26] Droplet size distributions have also been collected experimentally and are discussed elsewhere.[9] The effects of these parameters on the contactor experiments are discussed.

Experimental Methods

Diffusion and partition coefficients

Diffusion Coefficients. Diffusion constants were measured in the aqueous and organic phases using a side-by-side diffusion cell (PermeGear, Hellertown, PA, model #5G-00-00-15-07), which has been described elsewhere.[10,11] A membrane was placed between two 7-mL glass cells. Each glass cell was continuously stirred by a magnetic stir bar. With both cells filled with solvent, a small volume of solvent was removed from one of the cells, which was then replaced with the same volume of a dilute solution of the solute of interest. The concentration in one of the cells (the unadulterated cell) was then monitored by continuous UV-vis spectroscopy using an Ocean Optics spectrometer (QE6000) and a light source (LED Dolan Jenner LMI-6000). Flow through the membrane is sensitive to pressure differences in the cells, thus the cells were left open for approximately an hour to equalize pressure and then gently taped with a piece of scotch tape to prevent evaporation. The membrane was calibrated by performing the measurement using a compound with a known diffusion constant.

In the aqueous diffusion experiments an acrylic-nylon membrane (Gelman Pall Versapor-800, 0.8 μm, 47 mm diameter, PN 66401) was used to separate the half-cells. rhodamine B (Sigma-Aldrich), 500 μL of 13.4 μM was added to the 7 mL half-cell as the membrane-calibration solute. Rhodamine B has strong UV-vis absorption at 550 nm, and its diffusion constant has been determined to be $4.2 \pm 0.3 \times 10^{-10}$ m^2/s at pH = 2 to 9.5, ionic strengths < 0.1 M, and concentrations < 10 μM.[27] The solvent for the membrane-calibration was 0.008 M KHP buffer set to a pH of 5.75; the absorbance, diffusion, and complexation of rhodamine B, fluorescein, and xylenol orange are sensitive to pH. As a calibration check, we performed diffusion experiments using fluorescein (Fluka). A 500-μL aliquot of 400-μM fluorescein was added to the 7-mL half-cell containing 0.008 M KHP buffer. Absorbance was measured vs. time at 489.68 nm, which gave a diffusion constant $D = 3.9 \pm 0.6 \times 10^{-10}$ m^2/s consistent with experiments by Perale et al.[28] but below other literature values $4.2 - 6.4 \times 10^{-10}$ m^2/s.[29,30] With nearly all of the compounds of interest we observed anomalous absorbance trends over long periods of time (weeks), which we attribute to slow degradation of the organic dyes, and/or aggregation.[29]

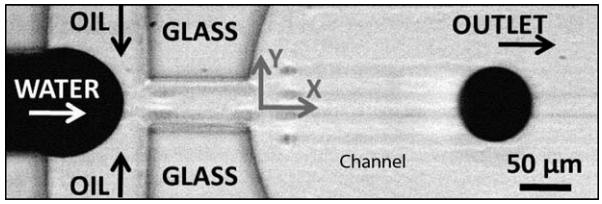

Figure 1. Flow focusing geometry showing aqueous drops (dark) being produced in dodecane.

Orifice sizes are 50 and 100 µm, with all other dimensions being equal. The channel depth is 100 µm.

For the organic diffusion experiments, a PFTE membrane (Pall Zelfluor, 0.5 μm, 47 mm diameter, PN P5PQ047) with the cellulose backing material removed was used to separate the two half-cells. Dimethyl yellow (Fluka) was used as the membrane-calibration solute with a diffusion constant of 9.9×10^{-10} m^2/s.[31,32] A 1500-μL aliquot of 100-μM dimethyl yellow was added to the high side cell, absorbance was taken at 416.91 nm. The diffusion constant for the Nd-TTA-TBP complex was determined by first mixing equal volumes of 0.05 M $Nd(NO_3)_2$(aq) and 0.2 M HTTA + 0.1 M TBP in dodecane. A 1-mL aliquot of the Nd-laden organic phase was then pipetted into a clean solution of 0.2 M HTTA + 0.1 M TBP in dodecane as the matrix medium. Absorbance was then measured vs. time at 580.95 nm.

Partition Coefficients. Partition coefficients were determined placing volumes (3–30 mL) of the organic and aqueous phase in contact in bottles that were gently shaken on a shaker table for at least 1 h. Although we did not perform a time-dependent study examining the approach to equilibrium, an equilibrium time of 1 h is consistent with the time required in previous work for similar systems.[12,33] The aqueous phase was then separated and sampled for ICP-OES analysis (Perkin Elmer Optima 8000). In the organic phase, we combined dodecane (Sigma-Aldrich, >99 %), HTTA (Sigma-Aldrich, St. Louis, MO), and TBP (Sigma-Aldrich). In the aqueous phase, we used two formulations of xylenol orange, neodymium(III) nitrate, and KHP corresponding to the microfluidic experiments and the contactor experiments, respectively.

Drop production and flow visualization

Homogeneous droplets were produced in a flow-focusing microfluidic device shown in Figure 1.[34] The device consisted of a cross geometry with the continuous phase fluid flowing past the dispersed phase, generating a jet which breaks up into drops due to capillary instability. Glass chips were purchased from Translume (Ann Arbor, MI) and were made hydrophobic using a 2 vol % octadecyltrichlorosilane (OTS) (Sigma-Aldrich, St. Louis, MO, > 90% pure) in hexadecane (Sigma-Aldrich, St. Louis, MO, anhydrous > 99%) wash. Chip orifice widths were 50 and 100 μm, and the chip

Table 1. Aqueous Diffusion Coefficients

Species	Medium	Diffusion Coefficient (m^2/s)
Nd(XO)(aq)	0.2 M KHP buffer at pH 5.5	$2.3 \pm 0.2 \times 10^{-10}$
H_3XO(aq)	0.2 M KHP buffer at pH 5.5	$3.0 \pm 0.2 \times 10^{-10}$
Nd^{3+}(aq)	0.01M NaAc buffer at pH 5.5	$7.0 \pm 0.7 \times 10^{-10}$

depth was always 100 μm. The continuous fluid was dodecane (Sigma-Aldrich, St. Louis, MO, >99% pure). Flow rates were specified using syringe pumps (Harvard Apparatus, PhD 22/2000, Holliston, MA), which were calibrated gravimetrically using a balance (Mettler Toledo, XS1003S, Columbus, OH). Continuous fluid flow rates were varied from 1 to 5 mL/h. Droplet production in a similar system was discussed previously, including control of size and frequency of droplets.[34]

Flow was visualized using an inverted microscope (Leica DM IRB, Germany), and recorded using a high speed CCD camera (Phantom v 9.1, Vision Research, Wayne, NJ), with frame rates as high as 5000 frames per second. Distances are calibrated using Klarmann Rulings, (Litchfield, NH) KR-868 reticules.

Mass transfer to droplets in microfluidic chip

The extraction of neodymium (Nd^{3+}) from aqueous droplets to dodecane using the complexant HTTA (Sigma-Aldrich, St. Louis, MO) and ligand TBP (Sigma-Aldrich, St. Louis, MO) was chosen as a model mass-transfer system.[12,35] The aqueous phase also included xylenol orange (XO, Sigma-Aldrich, St. Louis, MO) as an indicator for Nd^{3+}. In all cases, the aqueous droplet fluid was 3.2 mM $NdNO_3$ (Sigma Aldrich, St. Louis, MO), 0.01 M xylenol orange, and was buffered at pH = 5.5 using 0.2 M potassium hydrogen phthalate (KHP, Acros Organics, NJ). The continuous dodecane phase had varying concentrations of TBP and HTTA as specified. Aqueous solution concentrations were verified using ICP-OES.

Uncomplexed xylenol orange absorbs light at 430 nm, whereas the XO-Nd complex absorbs at 590 nm.[36] Therefore, by illuminating the microfluidic chip only at 590 nm using a 70 mW LED (M590L2, Thor Labs, Newton, NJ), the intensity of the resulting image could be correlated with the XO-Nd concentration. Light intensity was captured using a Phantom V9.1 camera at 2000 fps as well as a photodiode (APD110A, Thor Labs, Newton, NJ). The photodiode signal was recorded with a National Instruments multifunctional data acquisition device (NI-USB-6366) and LabVIEW Signal Express software at 10^6 Hz (National Instruments, Austin, TX). The photodiode signal represents the average intensity of an image of a drop with a field of view that is approximately 1.5 times the maximum drop size obtained in the experiments. Drops were produced at a frequency such that only one drop was in the imaging area at a time. The resulting signal was periodic as drops moved in and out of the photodiode field of view, oscillating between dark values representing the intensity of drop-containing images and bright values representing the intensity of the background. The log of the ratio between the drop intensity to the background intensity is then a quantitative measure of the Nd-XO complex concentration by Beer's law.

For both photodiode and camera methods, calibration curves relating the log of the light intensity to the XO-Nd complex concentration were created by imaging droplets of six different concentrations ranging from 0 to 3.2 mM Nd-XO through pure dodecane. Calibration curves were linear, with R^2 values of 0.986 (photodiode) and 0.995 (camera). These curves are included in Supporting Information Appendix A (online). In the case of the photodiode, the calibration curves were specific to a given drop size, as the photodiode measured light over an area 1.5 times the drop size. In all cases, the concentrations were obtained with the highest accuracy when the drops spanned the entire depth of the chip, since the light path length in this case was known and consistent. Thus, drops with diameters larger than the channel depth were primarily used in this work, such that drops maintained a disk-like shape rather than a spherical shape. The production of these drops is discussed elsewhere.[34]

To obtain the change of concentration in the drops as they traveled down the channel of the microfluidic chip, images were taken along the length of the microfluidic chip channel (see Figure 1). Image locations are known through use of a motorized stage (ProScan, Prior Scientific, Cambridge, UK). Droplet velocities and sizes are measured from the images obtained through the Phantom camera. Along with the chip location information, these data can be translated to a diffusion time. The average concentration in the drops is reported using more than 2×10^6 measurements using the photodiode. A two-dimensional image of the concentration throughout a drop can also be obtained by relating the camera image intensity to concentration using the calibration curve mentioned previously.

Observations of the fluid circulation pattern that develops within the droplets are published elsewhere.[26] The droplet fluid exhibits a vortex in the horizontal plane, parallel to the microfluidic chip. Fluid is driven backward toward the trailing end of the droplet along the drop edges and returns to the front of the drop along the centerline. Large, surface active molecules TBP and HTTA were not seen to influence the interfacial or vortex motions.[37]

Mass transfer in centrifugal contactor

Mass transport experiments were conducted in a CINC V2 contactor, operated at 3200 rpm, using a diluted version of the formulation used for the microfluidic experiments. The aqueous phase consisted of 1.8×10^{-4} M Nd + 3.6×10^{-4} M xylenol orange in 0.1 M KHP buffer set to pH = 5.5. The organic phase consisted of 0.1 M HTTA + 0.1 M TBP in dodecane diluted with various amounts of dodecane. The flow rates of the aqueous and organic phases through the contactor were 3 mL/min and 1 mL/min, respectively. Flow rates were verified using a stop watch and a graduated cylinder. The aqueous outlet of the contactor was sampled periodically for later analysis by ICP-OES. The aqueous phase was recycled through the contactor and the organic phase was discarded after one pass through the contactor.

Results and Discussion

Diffusion and partition coefficients

Diffusion Coefficients. The diffusion coefficients in the aqueous phase are given below in Table 1. The diffusion constants for Nd(XO)(aq) and the H_3XO(aq) were determined in 0.2 M KHP buffer. For the bare Nd^{3+} ion, this was not possible as Nd^{3+} tends to form a solid phase with KHP in the absence of the XO complexant, hence a lower-concentration (0.01 M) sodium-acetate buffer was used; the

Table 2. Organic Diffusion Coefficient

Species	Medium	Diffusion Coefficient (m^2/s)
Nd-HTTA-TBP	0.2 M HTTA + 0.1 M TBP in Dodecane	$3.7 \pm 0.4 \times 10^{-10}$

pH in this case matched the pH used in the mass-transport experiments. The diffusion constant for the Nd-HTTA-TBP complex in the organic phase is given in Table 2.

Partition Coefficients. Partition data is shown below in Tables 3 and 4 for the microfluidic chip and contactor relevant experimental formulations, respectively. We also calculated a distribution value $D_{o,aq}$ as the total concentration of neodymium in the organic phase divided by the total concentration of neodymium in the aqueous phase. A fit to the standard complex given in Eq. 1 was attempted; however looking at the data, it is clear that the concentration of Nd in the organic phase depends in a complicated way on TTA concentration rather than cubically, most likely due to multiple complexes acting in solution.

Droplet concentration and mass-transfer coefficients in the microfluidic chip

The concentration of Nd-XO complex in the droplets was recorded as the droplets traveled down the chip outlet channel for various continuous fluid flow rates and TBP and HTTA concentration. An example image of a drop undergoing mass transfer in the microfluidic chip is shown in Figure 2, which shows a droplet initially containing 3.62 mM Nd^{3+}, 0.01 M xylenol orange, and 0.2 M KHP traveling in a continuous dodecane liquid containing 0.2 M HTTA and 10^{-2} M TBP flowing at 1.5 mL/h. The false color represents the concentration of Nd-XO complex in the aqueous phase. This image was taken with the Phantom camera, as discussed in Section Experimental Methods. As expected, the drop is depleted of Nd-XO complex at the outer edges due to mass transfer. The depleted material is swept around the droplet edges and brought back to the front of the droplet by a vortex pattern that develops due to the shear in the microfluidic channel.[26] The highest concentration of complex is found at the centers of the vortices. Drops produced using other flow rates are more homogeneous in concentration, suggesting regimes of both kinetic and diffusion limited mass transfer were observed. This will be discussed in the Sections Kinetically Controlled Mass-Transfer Regime and Diffusion Controlled Mass-Transfer Regime.

Kinetically Controlled Mass-Transfer Regime. When the HTTA concentration in the continuous phase was less than 0.004 M, the mass transfer at the droplet surface was slow compared to the diffusion of Nd in the droplet. Assuming that the droplet is well mixed and the concentration of Nd^{3+} is constant in the outer fluid, a mass-transfer balance for the concentration of Nd^{3+} in the aqueous phase, C, at time t can be written for a droplet of surface area, A, and volume, V

$$k_{eff}A(C - D_{o,aq}^{-1}C_o)dt = -VdC \tag{2}$$

where k_{eff} is the first-order mass-transfer reaction rate. Since the flow rate of continuous fluid is always 100 times greater than that of the droplet fluid, the quantity $D_{o,aq}^{-1}\ C_o$, the partition coefficient times the Nd^{3+} concentration in the dodecane is approximated to be zero. Upon integrating this equation and simplifying the area to volume ratio of a sphere, an expression for the effective mass-transfer coefficient k_{eff} can be found

$$\frac{-6k_{eff}t}{d} = \ln\left(\frac{C}{C_i}\right) \tag{3}$$

Here, C_i is the initial concentration of Nd^{3+} in a drop with diameter d. The effective mass transfer coefficient combines the mass-transfer rate at the liquid–liquid interface as well as the mass-transfer rate across any concentration gradients in the fluid.

Using this simplified model, k_{eff} was found for a range of TBP and HTTA concentrations. Figure 3 displays representative data for four separate cases. Plots of $\ln(C/C_i)$ vs. t/d were linear. Values of R^2 corresponding to the linear fit used to find k_{eff} are reported. As shown in Figure 3, the continuous fluid flow rate (Q_c) did not impact the mass-transfer coefficient. The observations that $\ln(C/C_i)$ was linear with t/d

Table 3. Partition Data for the Microfluidic-Chip Relevant Experiments

$[HTTA]_{initial,o}$ (mol/L)	$[TBP]_{initial,o}$ (mol/L)	$[Nd]_{eq,o}$ (mol/L)	Vol aq (mL)	$D_{o,aq} = [Nd]_{eq,o}/[Nd]_{eq,aq}$ (dimensionless)
0.2	0.3	3.17×10^{-3}	30	4.81×10^{3}
0.2	0.3	3.17×10^{-3}	30	5.55×10^{3}
0.2	0.1	3.16×10^{-3}	30	3.04×10^{2}
0.2	0.01	3.15×10^{-3}	30	1.70×10^{2}
0.2	0.01	3.15×10^{-3}	30	1.65×10^{2}
0.004	0.0025	8.02×10^{-4}	30	3.39×10^{-1}
0.004	0.0025	8.13×10^{-4}	30	3.45×10^{-1}
0.002	0.0025	6.17×10^{-4}	30	2.42×10^{-1}
0.002	0.0025	6.40×10^{-4}	30	2.53×10^{-1}
0.002	0.01	6.48×10^{-4}	30	2.57×10^{-1}
0.002	0.01	6.47×10^{-4}	30	2.57×10^{-1}
0.002	0.005	6.16×10^{-4}	30	2.42×10^{-1}
0.002	0.005	6.48×10^{-4}	30	2.57×10^{-1}
0.004	0.0025	2.73×10^{-4}	3	6.22×10^{-1}
0.002	0.0025	1.80×10^{-4}	3	1.31×10^{-1}
0.002	0.01	2.46×10^{-4}	3	3.45×10^{-1}
0.002	0.005	2.31×10^{-4}	3	2.70×10^{-1}

Here the initial $[Nd(XO)]_{aq} = 3.2$ mM, the xylenol orange concentration was 0.01 M and the matrix solution was 0.2 M KHP buffer pH = 5.45. The volume of the organic phase was 30 mL. The volume of the aqueous phase is as given in the table.

Table 4. Partition Data for the Contactor Relevant Experiments

$[HTTA]_{initial,o}$ (mol/L)	$[TBP]_{initial,o}$ (mol/L)	$[Nd]_{eq,o}$ (mol/L)	$D_{o,aq} = [Nd]_{eq,o}/[Nd]_{eq,aq}$
1.00×10^{-1}	1.00×10^{-1}	1.79×10^{-4}	1.21×10^{2}
1.00×10^{-1}	1.00×10^{-1}	1.79×10^{-4}	1.35×10^{2}
5.00×10^{-2}	5.00×10^{-2}	1.80×10^{-4}	4.56×10^{2}
2.50×10^{-2}	2.50×10^{-2}	1.80×10^{-4}	5.73×10^{2}
2.00×10^{-2}	2.00×10^{-2}	1.78×10^{-4}	8.31×10^{1}
2.00×10^{-2}	2.00×10^{-2}	1.78×10^{-4}	8.90×10^{1}
1.11×10^{-2}	1.11×10^{-2}	1.71×10^{-4}	1.96×10^{1}
1.11×10^{-2}	1.11×10^{-2}	1.71×10^{-4}	1.97×10^{1}
9.09×10^{-3}	9.09×10^{-3}	1.67×10^{-4}	1.26×10^{1}
9.09×10^{-3}	9.09×10^{-3}	1.67×10^{-4}	1.26×10^{1}
9.09×10^{-3}	9.09×10^{-3}	1.35×10^{-4}	3.01×10^{0}
9.09×10^{-3}	9.09×10^{-3}	1.72×10^{-4}	2.28×10^{1}
4.76×10^{-3}	4.76×10^{-3}	7.31×10^{-5}	6.85×10^{-1}
4.76×10^{-3}	4.76×10^{-3}	1.48×10^{-4}	4.71×10^{0}
3.23×10^{-3}	3.23×10^{-3}	6.52×10^{-5}	5.68×10^{-1}
3.23×10^{-3}	3.23×10^{-3}	1.51×10^{-4}	5.17×10^{0}

Here the initial $[Nd(XO)]_{aq} = 1.8 \times 10^{-4}$ M, the xylenol orange concentration was 3.6×10^{-4} M, and the matrix solution was 0.1 M KHP buffer pH = 5.45.

and the lack of dependence on Q_c are consistent with a kinetically limited process.

Table 5 lists the results for k_{eff} for runs in the kinetically controlled regime. Also reported in Table 5, the Reynolds number defined for the continuous fluid flow through the outlet channel with width w, $Re = \rho_c Q_c / w\mu_c$, showing that the flow is always laminar. The drop-scale Reynolds number, using the parameters given in Table 5 yields $Re = \rho_d V_d d/\mu_d \sim 1$. The drop velocity V_d, and the relative velocity of the drop with respect to the maximum velocity of the fluid V_{rel} are also given. The Peclet number, Pe, is defined for the drop as $Pe = V_{rel}\, d/(4D)$, where the diffusion coefficient for the Nd(XO)(aq) complex, D, is that given in Table 1. Here the length scale for diffusive transport is assumed to be one-fourth of the drop diameter, d, or approximately the distance to the center of the vortex observed in Figure 8 of Roberts et al.[26] The Peclet number $Pe \sim 100$, confirming that convection in the droplet is much faster than diffusion across streamlines. The values of k_{eff} shown in Table 5 indicate that the mass-transfer rate was roughly first-order with

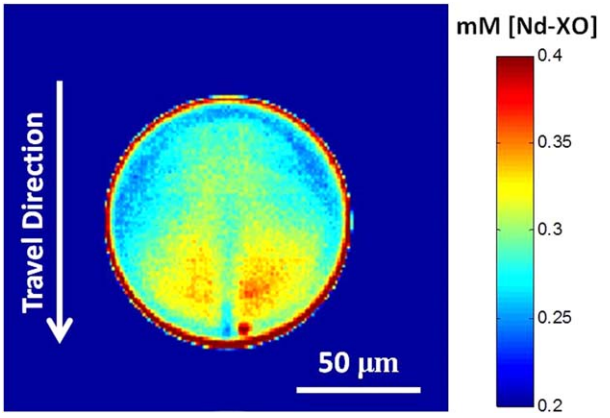

Figure 2. Aqueous drop in the microfluidic channel, approximately 0.5 cm from the orifice.

Here, color represents the concentration of the neodymium-xylenol orange complex. [Color figure can be viewed in the online issue, which is available at wileyonlinelibrary.com.]

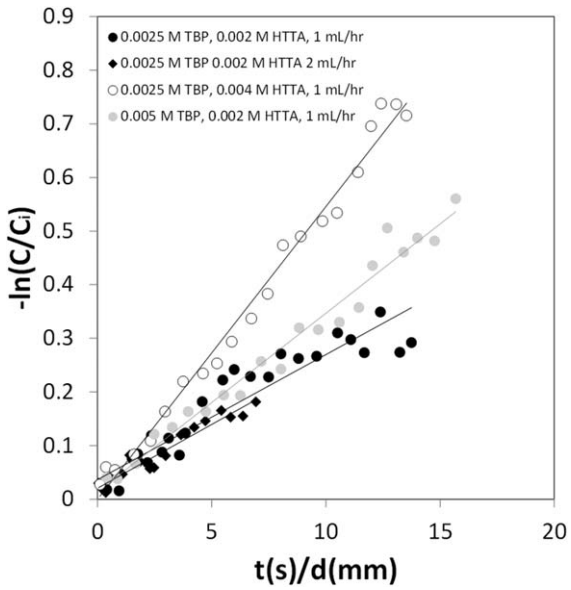

Figure 3. Concentration as a function of time for (●) 0.0025 M TBP, 0.002 M HTTA, $Q_c = 2$ mL/h; (◆) 0.0025 M TBP, 0.002 M HTTA, $Q_c = 2$ mL/h; ○) 0.0025 M TBP, 0.004 M HTTA, $Q_c = 2$ mL/h, (●) 0.005 M TBP, 0.002 M HTTA, $Q_c = 2$ mL/h.

HTTA concentration and was only weakly dependent on the TBP concentration; however, the presence of TBP was necessary to obtain mass transfer and prevent the formation of a solid phase (presumably an Nd-TTA phase) in the organic liquid. The assumption that the droplets are well mixed can be tested by calculating the mass-transfer Biot number, defined as $Bi = k_{eff} d/4D$, (given in Table 5) with the diffusion constant for the Nd(XO)(aq) complex taken from Table 1. The value of Bi for all cases in Table 5 is greater than one, indicating that the kinetic transport to the drop is faster or at least comparable to the diffusive transport within the drop. This suggests that for rigorous determination of the mass-transfer coefficient a mixed kinetic-diffusion model may be more appropriate. The Biot number does not take into account effects of Taylor dispersion, which would increase the diffusion rate within the drop due to shear. It also assumes that the droplet shape is purely spherical within the channel and that the characteristic length scale for diffusion in the droplet is $d/4$. If thin continuous liquid boundary layers between the droplet and the channel wall become depleted of species, this is also not accounted for.

Diffusion Controlled Mass-Transfer Regime. When the HTTA concentration in dodecane was increased to ~0.2 M, the mass-transfer kinetics at the drop interface became diffusion limited. Looking at Figure 2 (organic phase HTTA concentration = 0.2 M), at the edges of the drop is a false ring of high complex concentration, which is an artifact of imaging the oil–water interface. At the edges of the drop and at the centerline, the neodymium concentration is depleted. This corroborates the circulation pattern described in Roberts et al.,[26] where the aqueous liquid travels in symmetric two vortices. From the figure, diffusion has not homogenized the neodymium concentration throughout the drop and therefore the mass transfer under these conditions is diffusion limited. Figure 4 shows the fraction of Nd^{3+} extracted from a drop vs. time, nondimensionalized by a

Table 5. Parameters Obtained for Microfluidic Reaction-Limited Mass-Transfer Experiments

Continuous Fluid										
TBP (mol/L)	HTTA (mol/L)	Q_c (mL/h)	V_d (mm/s)	V_{rel} (mm/s)	d (mm)	k_{eff} (mm/s)	R^2	Re	Pe	Bi
0.0025	0.002	2	15	−4.3	0.084	3.9×10^{-3}	0.88	0.62	392	3.19
0.0025	0.002	4	33	−5.7	0.083	4.0×10^{-3}	0.93	1.24	514	3.22
0.0025	0.004	2	16	−3.1	0.084	9.1×10^{-3}	0.99	0.62	283	7.48
0.0025	0.004	4	34	−4.4	0.080	7.3×10^{-3}	0.97	1.24	382	5.77
0.005	0.002	2	14	−5.1	0.084	5.6×10^{-3}	0.97	0.62	465	4.56
0.005	0.002	4	31	−7.7	0.083	5.9×10^{-3}	0.95	1.24	694	4.80
0.01	0.002	4	33	−5.6	0.083	5.3×10^{-3}	0.93	1.24	505	4.29
0.01	0.002	2	15	−4.5	0.085	5.3×10^{-3}	0.99	0.62	415	4.41

characteristic time for diffusion, $\tau = 4Dt/d^2$, with the diffusion constant for the Nd(XO)(aq) complex taken from Table 1. The mass transfer of all cases is equivalent, irrespective of the TBP concentrations in the dodecane. For comparison, the Kronig-Brink solution for mass transfer from a perfectly circulating sphere translating through a quiescent fluid is also included.[21,38] The Kronig-Brink solution assumes a perfectly symmetrical flow pattern within the drop. Since the Kronig-Brink solution contains more circulation than the observed flow, the observed mass transfer is slower. From these microfluidic mass-transfer experiments, the boundary between kinetically limited mass transfer and diffusion limited mass transfer was found to occur at $Bi >\sim 7.5$.

The observation that the TBP concentration did not influence the mass transfer in the diffusion limited regime is additional evidence that TBP does not affect the mobility of the liquid–liquid interface significantly.[26] If TBP caused slip at the dodecane–water interface, the circulation pattern within the droplet would have been altered and the relevant diffusion length would have changed.[24] Within the experimental capabilities, this was not observed.

Mass transfer in the centrifugal contactor

A simple model that includes the contactor, a well-stirred aqueous reservoir, and the piping between the reservoir and the contactor is given here for the purpose of understanding the contactor mass-transfer results and for the purpose of comparing mass-transfer rates to the microfluidic chip experiments. The model is depicted in Figure 5, where C_r is the concentration of Nd^{3+} in the aqueous reservoir and in the fluid leaving the reservoir, $C_{r,i}$ is the concentration of Nd^{3+} in the aqueous fluid entering the reservoir, $C_{c,o}$ is the concentration of Nd^{3+} in the aqueous fluid exiting the contactor, and $C_{c,i}$ is the concentration of Nd^{3+} in the aqueous fluid entering the contactor. These concentrations are related by

$$C_{c,i}(t) = C_r(t - t_i) \tag{4}$$

$$C_{r,i}(t) = C_{c,o}(t - t_o) \tag{5}$$

where t_i and t_o are the lag times required for the fluid to travel from the reservoir exit to the contactor entrance and from the contactor exit to the reservoir entrance, respectively. The concentration of Nd in the fluid exiting the contactor can be calculated using a model based on Eq. 3

$$C_{c,o}(t) = C_{c,i}(t - t_c)e^{-(6k_{eff}t_c/d)} \tag{6}$$

where t_c is the time spent in the contactor (which is estimated below). Equations 4–6 can be combined to determine $C_{r,i}(t)$ in terms of $C_r(t)$

$$C_{r,i}(t) = C_r(t - t_l)e^{-(6k_{eff}t_c/d)} \tag{7}$$

where t_l is the total trip time around the aqueous loop, $t_l = t_i + t_c + t_o$. With Eq. 7, we can write the following mass balance equation

$$\frac{dC_r}{dt} = \frac{F}{V_r}\left[C_{r,i}(t) - C_r(t)\right] = \frac{F}{V_r}\left[C_r(t - t_l) - C_r(t)e^{-(6k_{eff}t_c/d)} - C_r(t)\right] \tag{8}$$

where F is the volumetric flow rate of the aqueous phase (3 mL/s), and V_r is the aqueous-reservoir volume ($\approx$ 100 mL). Nondimensionalizing time by t_l, C_r by $C_r(t=0)$ in Eq. 8 and solving yields the following relation

$$k_{eff} = \frac{d\left(K - \ln\left(1 - \frac{KV_r}{Ft_l}\right)\right)}{6t_c} \tag{9}$$

Here K is the slope of $-\ln(C_{r,i}(t)/C_r(t=0))$ vs. t/t_l. The mean drop diameter, d, was estimated to be 100 μm,[9] however, there is a distribution of drop sizes in the contactor. The drop sizes in Wyatt et al.[9] were measured for PDMS in water. A separate experiment was performed for dodecane in water which obtained similar results; these data are available on request. The residence time in the contactor t_c was estimated by assuming the drops make a plug-flow descent

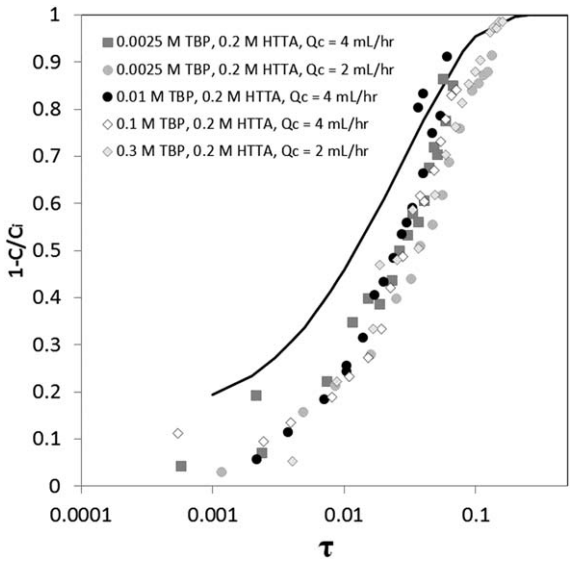

Figure 4. Fraction of Nd^{3+} transferred vs. dimensionless time for diffusion limited experimental cases (symbols).

The Kronig-Brink solution for a perfectly circulating sphere in plug flow is shown for comparison (−).

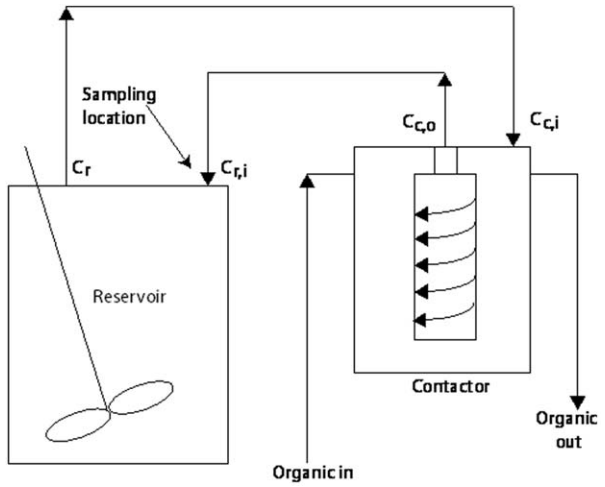

Figure 5. Schematic description of contactor-experiment.

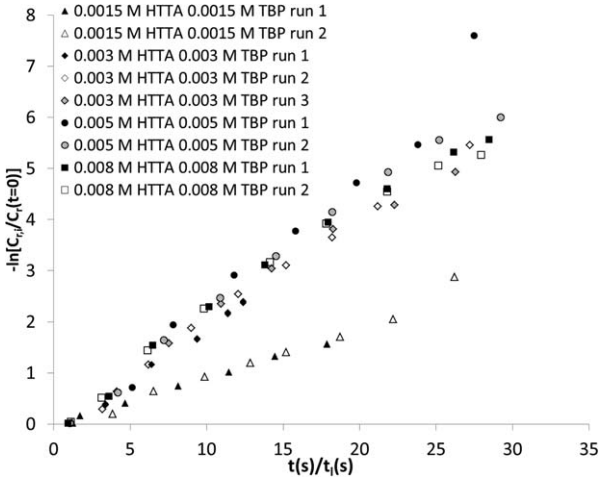

Figure 6. Aqueous Nd concentration vs. time normalized by total trip time around the loop on the outlet of the contactor for various concentrations of HTTA and TBP.

along the contactor. Estimating the total liquid volume in the contactor from Wyatt et al.[9] to be $V_c \approx 14$ mL, and given the total (organic + aqueous) flow rate of $F_{total} = 4$ mL/s yields $t_c = V/F_{total} = 3.5$ s.

A plot of $-\ln(C_{r,i}/C_r(t=0))$ vs. t/t_l is shown in Figure 6. The time lag around the aqueous loop, t_l, was roughly estimated using a stop watch while the contactor was initially empty and was found to be ≈ 15 s. At concentrations of 0.003 M HTTA + 0.003 M TBP and above, the curves collapse, which we hypothesize indicates that diffusion is dominating over chemical kinetics. If thermodynamic control were dominant, the curve slopes would continue to increase with increasing HTTA concentration. Table 6 gives the slopes of the curves in Figure 6. The resulting values of k_{eff} from Eq. 9 are also shown in Table 6, which are in reasonable agreement with the values given in Table 5 for similar concentrations of HTTA and TBP.

Also shown in Table 6 is the Biot number, redefined with a characteristic length scale of $d/2$ instead of $d/4$, and using the diffusion coefficient D for the organic Nd-TTA-HTP complex taken from Table 2; in the contactor the organic phase was the dispersed phase.[9] The $d/2$ length scale arises from the expectation that there is a single vortex within each drop,[39] unlike the microfluidic chip experiments. The boundary between kinetic and diffusion Bi number appears to be between 2 and 5, in reasonable agreement with the microfluidic results. The flow regime in the contactor (see Wyatt et al.[9]) can be estimated by taking the inner rotor speed (3200 RPM) and the inner rotor diameter (50.8 mm) to obtain the linear velocity of the inner rotor to be ~ 8.5 m/s. The gap between the inner rotor and the outer wall of the contactor was 6.35 mm. Thus a lower bound on the shear rate that the drops experience $\gamma \sim$ (8.5 m/s)/(6.35 mm) $\sim 10^3$ s^{-1}. Then calculating the $Pe = \gamma d^2/(4D) \sim 6 \times 10^4$, with D taken from Table 2 we find that diffusion is subdominant to convection. The Reynolds number based on the gap $Re = 5.4 \times 10^3$, based on an aqueous continuous phase ($\mu = 1$ cSt, $\rho = 1$ g cm^{-3}). On a drop scale ($d \sim 100$ μm), $Re = 900$ using the viscosity and density of water, and 500 using the viscosity and density of dodecane.

Conclusions

A study was performed to determine whether single-drop experiments in a microfluidic chip could be used to predict and understand the mass-transfer characteristics of a turbulent centrifugal contactor. To this end a model system was developed containing Nd(III) + xylenol orange in the aqueous phase buffered to pH = 5.5 with KHP, and dodecane + HTTA + TBP as the organic phase. Diffusion coefficients were measured for neodymium species complexed with xylenol orange in the aqueous phase, and for neodymium complexed with HTTA + TBP in dodecane. The partition coefficient between the total concentration of Nd(III) in the organic and aqueous phases was determined. Drop-scale microfluidic experiments were used to determine chemical concentrations of complexant that lead to kinetic vs. diffusion control. Laboratory scale centrifugal contactor experiments confirmed that both kinetic and diffusion limited mass-transfer regimes exist under realistic operating parameters. Furthermore the kinetic mass-transfer coefficients of the process corresponded well between the two experimental techniques, which was surprising given that Eq. 2 is phenomenological.

Although the macroscopic flow in the contactor is turbulent, on the drop scale, $Re \sim 500$, the flow is laminar, consistent with the microfluidic-chip experiments. Furthermore $Pe >> 1$ for both the contactor and microfluidic-chip experiments indicating that both experiments were either in the

Table 6. Effective Mass-Transfer Rate from the Contactor Experiments

HTTA (mol/L)	TBP (mol/L)	K (dimensionless)	Standard Deviation (dimensionless)	k_{eff} (mm/s)	Bi (dimensionless)
0.008	0.008	0.202	0.004	3.8×10^{-3}	4.6
0.005	0.005	0.246	0.04	4.9×10^{-3}	6.0
0.003	0.003	0.222	0.03	4.3×10^{-3}	5.2
0.0015	0.0015	0.0976	0.01	1.6×10^{-3}	2

kinetic or diffusion limited transport regimes, allowing comparison between the two experiments. The similar flow regime confirms that the microfluidic experiments offer the ability to see in real-time the mass transfer rather than average mass-transfer rates obtained in traditional column experiments. It is our hope that microfluidic environments could be used as a relatively simple and inexpensive approach for future studies of mass transfer from drops in contactors.

Literature Cited

1. Vedantam S, Wardle KE, Tamhane TV, Ranade VV, Joshi JB. CFD simulation of annular centrifugal extractors. *Int J Chem Eng*. 2012 2012:759397.
2. Deshpande KB, Zimmerman WB. Simulations of mass transfer limited reaction in a moving droplet to study transport limited characteristics. *Chem Eng Sci*. 2006;61(19):6424–6441.
3. Wardle KE, Lee T. Finite element lattice Boltzmann simulations of free surface flow in a concentric cylinder. *Comput Math Appl*. 2013; 65(2):230–238.
4. Kadam BD, Joshi JB, Koganti SB, Patil RN. Dispersed phase holdup, effective interfacial area and Sauter mean drop diameter in annular centrifugal extractors. *Chem Eng Res Design*. 2009;87(10):1379–1389.
5. Calabrese RV, Wang CY, Bryner NP. Drop breakup in turbulent stirred-tank contactors. Part III: Correlations for mean size and drop size distribution. *AIChE J*. 1986;32(4):677–681.
6. Wang CY, Calabrese RV. Drop breakup in turbulent stirred-tank contactors. Part II: Relative influence of viscosity and interfacial tension. *AIChE J*. 1986;32(4):667–676.
7. Leonard RA, Wygmans DG, McElwee MJ, Wasserman MO, Vandegrift GF. The centrifugal contactor as a concentrator in solvent extraction processes. *Sep Sci Technol*. 1993;28(1):177–200.
8. Cauwenberg V, Degreve J, Slater MJ. The interaction of solute transfer, contaminants and drop break-up in rotating disc contactors: Part I. correlation of drop breakage probabilities. *Can J Chem Eng*. 1997;75(6):1046–1055.
9. Wyatt NB, O'Hern TJ, Shelden B. Drop-size distributions and spatial distributions in an annular centrifugal contactor. *AIChE J*. 2013;59: 2219–2226.
10. Sanni SA, Hutchison P. Diffusivities and densities for binary liquid mixtures. *J Chem Eng Data*. 1973;18(3):317–322.
11. Chang P, Wilke CR. Some measurements of diffusion in liquids. *J Phys Chem*. 1954;59(7):592–596.
12. Farbu L, Alstad J, Auguston JH. Synergistic solvent extraction of rare-earth metal ions with thenoyltrifluoroacetone admixed with tributylphosphate. *J Inorg Nucl Chem*. 1974;36(9):2091–2095.
13. Lukaszewski MW, Zimmerman WBJ, Tennant MT, Webster MB. Application of inverse methods based algorithms to liquefied natural gas (LNG) storage management. *Chem Eng Res Des*. 2013;91:457–463.
14. Nichols KP, Pompano RR, Li L, Gelis AV, Ismagilov RF. Toward mechanistic understanding of nuclear reprocessing chemistries by quantifying lanthanide solvent extraction kinetics via microfluidics with constant interfacial area and rapid mixing. *J Am Chem Soc*. 2011;133(39):15721–15729.
15. Mary P, Studer V, Tabeling P. Microfluidic droplet-based liquid−liquid extraction. *Anal Chem*. 2008;80(8):2680–2687.
16. Xu JH, Tan J, Li SW, Luo GS. Enhancement of mass transfer performance of liquid-liquid system by droplet flow in microchannels. *Chem Eng J*. 200815;141(1-3):242–249.
17. Kumemura M, Korenaga T. Quantitative extraction using flowing nano-liter droplet in microfluidic system. *Anal Chim Acta*. 2006; 558(1-2):75–79.
18. Cristini V, Tan Y-C. Theory and numerical simulation of droplet dynamics in complex flows–a review. *Lab Chip*. 2004;4(4):257–264.
19. Gunther A, Jensen KF. Multiphase microfluidics: from flow characteristics to chemical and materials synthesis. *Lab Chip*. 2006;6: 1487–1503.
20. Teh S-Y, Lin R, Hung L-H, Lee AP. Droplet microfluidics. *Lab Chip*. 2008;8(2):198–200.
21. Kronig R, Brink J. On the theory of extraction from falling droplets. *Appl Sci Res*. 1951;2(1):142–154.
22. Johns LE, Beckmann RB. Mechanism of dispersed-phase mass transfer in viscous, single-drop extraction systems. *AIChE J*. 1966;12(1): 10–16.
23. Hudson SD, Cabral JT, Goodrum WJ, Beers KL, Amis EJ. Microfluidic interfacial tensiometry. *Appl Phys Lett*. 2005;87:081905.
24. Schwalbe JT, Phelan FRJ, Vlahovska PM, Hudson SD. Interfacial effects on droplet dynamics in poiseuille flow. *Soft Matter*. 2011; 7(17):7797–7804.
25. Horwitz EP, Kalina DG, Diamond H, Vandegrift GF, Schulz WW. The truex process - a process for the extraction of the transuranic elements from nitric-acid wastes utilizing modified purex solvent. *Solvent Extr Ion Exch*. 1985;3(1-2):75–109.
26. Roberts CC, Roberts SA, Nemer MB, Rao RR. Circulation within confined droplets in Hele-Shaw. *Phys Fluids*. 2014;26(3):032105.
27. Gendron P-O, Avaltroni F, Wilkinson KJ. Diffusion coefficients of several rhodamine derivatives as determined by pulsed field gradient-nuclear magnetic resonance and fluorescence correlation spectroscopy. *J Fluoresc*. 2008;18:1093–1101.
28. Perale G, Rossi F, Santoro M, Marchetti P, Mele A, Castiglione F, Raffa E, Masi M. Drug release from hydrogel: a new understanding of transport phenomena. *J Biomed Nanotechnol*. 2011;7(3):476–481.
29. Casalini T, Salvalaglio M, Perale G, Masi M, Cavallotti C. Diffusion and aggregation of sodium fluorescein in aqueous solutions. *J Phys Chem B*. 2011;115(44):12896–12904.
30. Galambos P. Two-phase dispersion in micro-channels [PhD Thesis]: University of Washington; 1998.
31. Yoo C-D, Kim S-C, Lee SH. Diffusion of a probe molecule in small liquid n-alkanes: a molecular dynamics simulation study. *Bull Korean Chem Soc*. 2008;29(8):1554–1560.
32. Park HS, Chang T. Diffusion of small probe molecule in oligomers. *J Chem Phys*. 2000;113(13):5502–5510.
33. Kassierer EF, Kertes AS. Synergic extraction of some lanthanides and transition metals by two bidentate chelating agents. *J Inorg Nucl Chem*. 1972;34:3221–3231.
34. Roberts CC, Rao RR, Loewenberg M, Brooks CF, Galambos P, Grillet AM, Nemer MB. Comparison of monodisperse droplet generation in flow-focusing devices with hydrophilic and hydrophobic surfaces. *Lab Chip*. 2012;12(8):1540–1547.
35. Sekine T, Dyrssen D. Solvent extraction of metal ions with mixed ligands—I. *J Inorg Nucl Chem*. 1964;26(1727):1727–1742.
36. Tonosaki K, Otomo M. Spectrophotometric determination of cerium(III) and some rare earths with xylenol orange. *Bull Chem Soci Jpn*. 1962;35(10):1683–1686.
37. Rao RR, Brotherton CM, Domino SP, Erickson LC, Grillet AM, Hughes LG, Jove-Colon CF, Lechman JB, Loewenberg M, Moffat HK, Nemer MB, Noble DR, John OHT, Roberts CC, Roberts SA, Shelden BW, Gregory J, Wyatt NB. Multiscale models of nuclear waste reprocessing : from the mesoscale to the plant-scale. Albuquerque, NM: Sandia National Laboratories; 2012. Report No.: SAND2012–9145.
38. Clift R, Grace JR, Weber ME. Bubbles, Drops, and Particles. New York, NY: Academic Press, 1978.
39. Bartok W, Mason SG. Particle motion in sheared suspension, VIII. Singlets and doublets of fluid spheres. *J Colloid Sci*. 1959;14:13–26.

Manuscript received Jan. 7, 2014, and revision received Mar. 26, 2014.